The Iron(III)-Catalyzed Oxidation of Ethanol by Hydrogen Peroxide: A Thermokinetic Oscillator

K.-P. Zeyer,[†,*] M. Mangold,[†] T. Obertopp,[‡] and E. D. Gilles[†,‡]

Max-Planck-Institut für Dynamik komplexer technischer Systeme, Leipziger Strasse 44, 39120 Magdeburg, Germany and Institut für Systemdynamik und Regelungstechnik Universität Stuttgart, Pfaffenwaldring 9, 70550 Stuttgart, Germany

Received: February 26, 1999; In Final Form: April 28, 1999

We present an experimental and theoretical study of a laboratory scale continuous flow stirred tank reactor (CSTR) in which the exothermic iron(III)-nitrate-catalyzed oxidation of ethanol with hydrogen peroxide to ethanal and acetic acid takes place. This reaction can display temperature and concentration oscillations when it is performed in a CSTR. A model is known in the literature, which is derived from a more detailed mechanism. We investigate the behavior of the system under different conditions using the volumetric flow of the cooling water as an experimental bifurcation parameter. The model is analyzed by one and two parameter continuation of stationary and periodic solutions. We characterize period doubling sequences to chaos, homoclinic orbits, and cross-shaped diagrams, which separate regions of oscillations and bistability.

1. Introduction

In contrast to isothermal oscillating systems, even first-order exothermic reactions with sufficiently high activation energies and reaction enthalpies can display periodic oscillations in temperature and material concentrations when they are performed in a continuous flow stirred tank reactor (CSTR).[1,2] Typical examples of thermokinetic oscillators are, for example, the decomposition of the dihydroperoxide of *m*-diisopropylbenzene,[3] the decomposition of dinitrogenoxide at a copperoxide contact,[4] the chlorination of methyl chloride in the gas phase,[5] the hydrolysis of acetyl chloride,[6] the oxidation of hydrogen by air at an aluminum oxide catalyst,[7] the oxidation of thiosulfate by hydrogen peroxide[8,9] the hydrolysis of 2,3-epoxy-1-propanol,[10] and the metal catalyzed decomposition of hydrogen peroxide.[11] Moreover, important industrial processes, such as the oxo synthesis (hydroformylation)[12] and the polymerization of styrene,[13] are also known to display thermokinetic oscillations under certain conditions. Hazardous states can occur when temperature oscillations with high amplitudes emerge suddenly after small changes of a control parameter[14] or when the system changes the stationary temperature of a given working point in a bistable region. Therefore, the knowledge of the reaction dynamics of such reactions is crucial for safe operating conditions.[15] On the other hand, operating the CSTR in an oscillating state may offer interesting possibilities to increase the yield of certain products.[16−18] In the literature many theoretical studies of the dynamics of exothermic reactions in a CSTR can be found,[19−21] but comparatively few experimental investigations have been published. Hafke and Gilles[22] demonstrated that the iron(III)-catalyzed oxidation of ethanol with hydrogen peroxide to ethanal and acetic acid can display temperature and concentration oscillations in a CSTR. They further derived a model, which is based on a more complex mechanism by applying quasi-stationary assumptions to intermediate species. The model describes the location of stationary states and Hopf bifurcation points well.

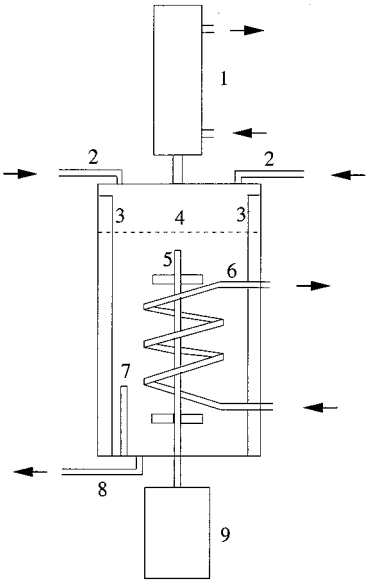

Figure 1. Experimental setup: (1) reflux condensor (height, 0.4 m; diameter, 0.1 m); (2) inlet tubes; (3) baffles, consisting of steel placed around the CSTR; (4) liquid surface; (5) stirrer (six blades; diameter, 4.8 cm); (6) cooling coil; (7) two heating elements (800 W each), only one is shown; (8) outflow; (9) stirring motor. The height of the reactor vessel is 0.3 m, and the inner diameter is 0.13 m.

The motivation of this work is to extend the previous studies by investigating the influence of parameter changes on the dynamics of the system. The experimental results are compared with model calculations, such as integration and continuation in one and two parameters.

2. Experimental Setup

All experiments are performed in a 3.5 L glass CSTR (Figure 1). The reactants enter the CSTR through the reactor top via

* Author to whom correspondence should be addressed.
† Max-Planck-Institut für Dynamik komplexer technischer Systeme.
‡ Institut für Systemdynamik und Regelungstechnik.

10.1021/jp990710v CCC: $18.00
Published on Web 06/16/1999

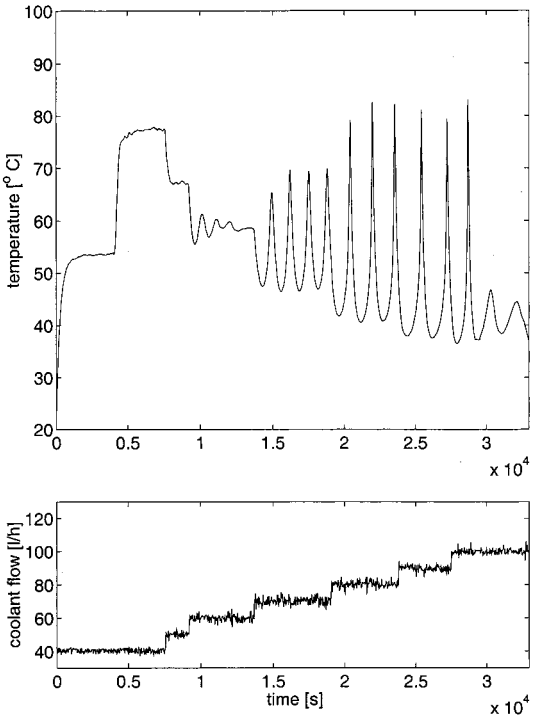

Figure 2. Experimental results: initial conditions (weight fractions) before dosing is turned on, $w_{CH_3CH_2OH} = 0.23$, $w_{cat} = 0.002$; weight fractions in dosing, $w_{H_2O_2,dos} = 0.09$, $w_{CH_3CH_2OH,dos} = 0.10$, $w_{cat,dos} = 0.02$; other conditions, $T_{dos} = 25.0$ °C, $T_{cool,in} = 8.0$ °C, $T_{amb} = 25.0$ °C, $N_{stirr} = 500$/min, $P_{heat} = 1600$ W; $t = 0-3975$ s: $\dot{q}_{dos} = 0$ L/h, $t = 3975-33000$ s: $\dot{q}_{dos} = 5.93$ L/h.

two feed streams (water/hydrogen peroxide and water/ethanol/iron(III) nitrate, respectively) driven by piston pumps. The ethanol (96 wt %, denatured with 1 wt % methyl ethylketone, Brenntag) and the hydrogen peroxide (35 wt %, Merck) are of technical purity whereas the iron(III) nitrate nonahydrate is of analytical grade (Merck). All educt solutions are prepared with destilled water. The reactor content is mixed by stirring (500 min^{-1}). It is possible to estimate the mixing time t_m by a correlation given in ref 23 as a function of the Reynolds number for different stirrers. For our reaction system we can approximate t_m to be of the order of 0.1 min, which is always small compared with the residence time of the CSTR. The liquid phase volume V_L is kept constant at 2.4 L via level control of the outflow at the reactor bottom. The reaction is equipped with two heating elements, 800 W each. Cooling is performed via a cooling coil (length, 3.0 m; inside diameter, 4 mm; outside diameter, 6 mm), which is made of steel. Additionally, a reflux condenser is placed on the top of the reactor (cooling surface 0.3 m^2, gas volume inside 1.1 L, volume of the cooling water 2.21 L). The actual reactor temperature T and the temperatures of the cooling inflow and outflow ($T_{cool,in}$ and T_{cool}) are measured by thermocouples. The concentration of hydrogen peroxide is evaluated offline by a reflectometric method (Merck Reflectoquant) from samples taken out of the reactor.

At the beginning of each experiment the reactor is filled with 2.4 L of an aqueous solution containing ethanol and iron(III) nitrate nonahydrate. The coolant flow is adjusted and the heating power as well as the stirrer are turned on. After a stationary state has been established, the dosing is activated.

3. Experimental Results

Figure 2 shows an experimental run where the reactor temperature T is depicted as a function of time. The volumetric

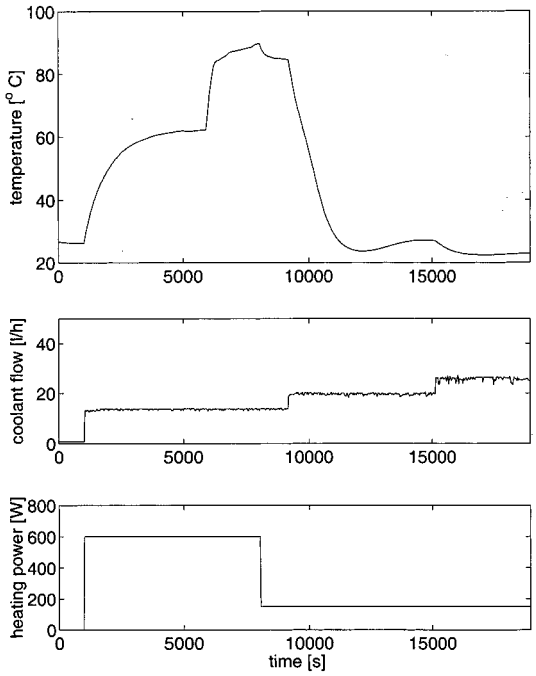

Figure 3. Experimental results: initial conditions (weight fractions) before dosing is turned on, $w_{CH_3CH_2OH} = 0.23$, $w_{cat} = 0.02$; weight fractions in dosing, $w_{H_2O_2,dos} = 0.06$, $w_{CH_3CH_2OH,dos} = 0.10$, $w_{cat,dos} = 0.0075$; other conditions, $T_{dos} = 22.0$ °C, $T_{cool,in} = 11.0$ °C, $T_{amb} = 22.0$ °C, $N_{stirr} = 500$/min; $t = 0-5870$ s: $\dot{q}_{dos} = 0$ L/h, $t = 5870-19000$ s: $\dot{q}_{dos} = 10.0$ L/h.

coolang flow $\dot{q}_{cool}$ is increased stepwise. At the beginning of the experiment the reactor is filled with an aqueous solutions containing 23 wt % ethanol and 0.2 wt % catalyst. Then the heating ($P_{heat} = 1600$ W), the stirrer ($N_{stirr} = 500$ min−1), and the coolant flow ($\dot{q}_{cool} = 40$ L/h) are turned on. After a constant temperature level of about $T = 54$ °C has been established in the CSTR, the dosing is started ($\dot{q}_{dos} = 5.93$ L/h). A steady state at $T = 77$ °C is found at $\dot{q}_{cool} = 40$ L/h. Running the reactor on this steady state the conversion of ethanol to acetic acid is high (reactive steady state), and therefore, only small concentrations of hydrogen peroxide are measured (mass concentration $\rho_{H_2O_2} = 0.75$ g/L). Increasing the coolant flow the temperature of the steady state decreases until oscillations with small amplitudes emerge at a Hopf bifurcation. Note that damped oscillationes are observed at $\dot{q}_{cool} = 60$ L/h close to the Hopf point. The oscillation amplitudes and periods increase when $\dot{q}_{cool}$ is increased further. Oscillations with high temperature amplitudes also manifest themselves by periodic changes in the amount of oxygen gas evolved, which can be clearly seen by the naked eye. At $\dot{q}_{cool} = 90$ L/h the reaction is so vigorous that the foaming solution reaches the condensor periodically at the maxima of the temperature oscillations. The region of oscillations ends at another Hopf bifurcation and gives way to steady states at low temperatures (extinguished steady state) at $\dot{q}_{cool} \geq 100$ L/h. On this branch of stationary behavior, the conversion of ethanol to ethanal and acetic acid is low and the oxidant hydrogen peroxide accumulates ($\rho_{H_2O_2} = 29.8$ g/L). This accumulation is a potential source of danger when the Hopf bifurcation is crossed in the reversed direction. Using higher weight fractions of hydrogen peroxide, $w_{H_2O_2,dos}$ in the feed stream results in a thermal runaway when this Hopf bifurcation point is reached by decreasing the coolant flow. In this case the temperature increase is very steep, and as a consequence, the gas evolution is so high and fast that a big part of the reacting solution is expelled through the condensor top. When the amount of hydrogen peroxide is decreased in the dosing, the size of the

region of oscillations becomes smaller and finally vanishes. At $w_{H_2O_2,dos} = 0.08$, for example, only very small temperature oscillations can be found, which is in accordance with the model calculations.

Nonoscillatory transitions between the reactive and the extinguished branch of steady states can be found when the amount of catalyst in the feed and the power of heating are diminished while the feed flow is increased. The experiment in Figure 3 shows a large temperature change from 87 to 27 °C when the flow of cooling water is slightly increased from $\dot{q}_{cool} = 15$ L/h to $\dot{q}_{cool} = 20$ L/h. Here again, the conversion of ethanol is high on the reactive steady state while it is low on the extinguished branch as can be seen from the measured concentrations of hydrogen peroxide at $\dot{q}_{cool} = 15$ L/h and $\dot{q}_{cool} = 20$ L/h ($\rho_{H_2O_2} = 0.78$ and 48 g/L, respectively). The temperature diminishes only slightly when the coolant flow is increased to $\dot{q}_{cool} = 25$ L/h (Figure 3).

4. Liquid Phase Model

The following reaction scheme was proposed by Hafke and Gilles:[22,26]

$$CH_3CH_2OH + H_2O_2 \xrightarrow{cat} CH_3CHO + 2\,H_2O \quad (-\Delta h_R)_1 = 302\ \text{kJ/mol} \quad (1)$$

$$CH_3CHO + H_2O_2 \xrightarrow{cat} CH_3COOH + H_2O \quad (-\Delta h_R)_2 = 389\ \text{kJ/mol} \quad (2)$$

$$H_2O_2 \xrightarrow{cat} 0.5\,O_2 + H_2O \quad (-\Delta h_R)_3 = 95\ \text{kJ/mol} \quad (3)$$

$$cat + CH_3COOH \rightarrow cat^*(-\Delta h_R)_4 = 0 \quad (4)$$

$$cat^* \rightarrow cat + CH_3COOH \quad (-\Delta h_R)_5 = 0 \quad (5)$$

The values $(-\Delta h_R)$ signify the reaction enthalpies under standard conditions ($T = 298.15$ K and $p = 101325.0$ Pa). The temperature dependence of these enthalpies as well as that of other physical properties, such as the densities or the heat capacities are evaluated using correlations given in the DIPPR catalogue.[24] Cat* denotes a catalytically inert acetatoiron(III) complex.[25] The dependence of the reaction rates on the temperature is described by the Arrhenius equation.

The rate expressions read

$$r_1 = k_1\, e^{-E_1/(RT)}\, c_{cat}\, c_{H_2O_2} \quad (6)$$

$$r_2 = k_2\, e^{-E_2/(RT)}\, c_{cat}\, c_{H_2O_2} c_{CH_3CHO} \quad (7)$$

$$r_3 = k_3\, e^{-E_3/(RT)}\, c_{cat} c_{H_2O_2} \quad (8)$$

$$r_4 = k_4\, e^{-E_4/(RT)}\, c_{cat} \sqrt{c_{CH_3COOH}} \quad (9)$$

$$r_5 = k_5\, e^{-E5/(RT)}\, c_{cat^*} \quad (10)$$

The preexponential factors and energies of activation are summarized in Table 1. Note that the rate of reaction 6 is independent of the ethanol concentration because ethanol is assumed to be in stoichiometric excess.[26]

TABLE 1: Preexponential Factors k_i and Energies of Activation E_i

i	k_i	E_i [kJ/mol]	ref
1	1.49480×10^{16} l mol^{-1} s^{-1}	105.50	26
2	1.95132×10^{20} l^2 mol^{-2} s^{-1}	126.20	26
3	6.66600×10^{14} l mol^{-1} s^{-1}	105.00	27
4	1.17637×10^{7} l$^{0.5}$ mol$^{-0.5}$ s^{-1}	55.69	26
5	3.83330×10^{4} s^{-1}	45.04	26

The mass balances read

$$\frac{dn_{H_2O}}{dt} = \dot{q}_{dos}\,(c_{H_2O,dos} - c_{H_2O}) + V_L(2r_1 + r_2 + r_3) \quad (11)$$

$$\frac{dn_{H_2O_2}}{dt} = \dot{q}_{dos}(c_{H_2O_2,dos} - c_{H_2O_2}) - V_L(r_1 + r_2 + r_3) \quad (12)$$

$$\frac{dn_{CH_3CH_2OH}}{dt} = \dot{q}_{dos}(c_{CH_3CH_2OH,dos} - c_{CH_3CH_2OH}) - V_L(r_1) \quad (13)$$

$$\frac{dn_{CH_3CHO}}{dt} = \dot{q}_{dos}(c_{CH_3CHO,dos} - c_{CH_3CHO}) + V_L(r_1 - r_2) \quad (14)$$

$$\frac{dn_{CH_3COOH}}{dt} = \dot{q}_{dos}\,(-c_{CH_3COOH}) + V_L(r_2 - r_4 + r_5) \quad (15)$$

$$\frac{dn_{cat}}{dt} = \dot{q}_{dos}\,(c_{cat,dos} - c_{cat}) - V_L(r_4 - r_5) \quad (16)$$

$$\frac{dn_{cat^*}}{dt} = \dot{q}_{dos}\,(-c_{cat^*}) + V_L(r_4 - r_5) \quad (17)$$

where $\dot{q}_{dos}$ denotes the volumetric feed flow and $c_{i,dos}$ signifies the feed concentrations.

The energy balance reads

$$(\Gamma + \Gamma_{ins})\frac{dT}{dt} = V_L \sum_{i=1}^{3} r_i(-\Delta h_R)_i + P_{heat} + P_{stirr} - \dot{q}_{dos}(\rho c_p)_{dos}\,(T - T_{dos}) - (UA)_{loss}\,(T - T_{amb}) - (UA)_{cool}(T - T_{cool,in}) \quad (18)$$

Γ and Γ_{ins} are the total heat capacities of the liquid phase and the inserts, respectively. P_{heat} is the power introduced by the two heating elements. P_{stirr} describes the power dissipated by the stirrer. ρ_{dos} and $c_{p,dos}$ denote the density and the specific heat capacity of the feed, respectively. T, T_{dos}, T_{amb}, and $T_{cool,in}$ are the reactor temperature, the temperature of the dosing, the ambient temperature, and the temperature of the cooling water at the inflow of the coil. $(UA)_{loss}$ and $(UA)_{cool}$ signify overall heat transfer coefficients, which describe the energy transfer to the ambient and to the cooling coil.

The dynamics of the wall of the cooling coil and the coolant were checked to be in the quasi-steady-state for the operating conditions. The heat transfer coefficients on the mixture and the coolant side were calculated on the basis of the correlations from the VDI−Wärmeatlas.[28] These correlations have been optimized with a parameter identification of dynamic experiments[29] at different stirrer speeds, coolant flows, and heating powers. The heat capacity Γ_{ins} of the inserts and the overall heat transfer coefficient $(UA)_{loss}$ to the ambient were determined in the same way to be 2290 J/K and 6.6 W/K, respectively.[14] The model is analyzed numerically by integration and continuation of steady states and periodic solutions using the simulation

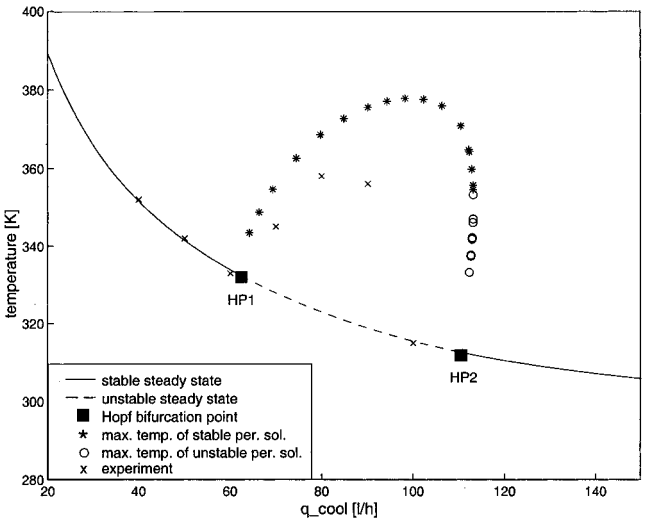

Figure 4. Comparison of the experimental results shown in Figure 2 with the theoretical results obtained by one-parameter continuation of stationary and periodic solutions (same conditions as those in Figure 2).

package DIVA.[30] It is also possible to determine the stability of stationary solutions and limit cycles via calculation of the eigenvalues of the Jacobi matrix and the Floquet multipliers, respectively.

5. Model Calculations

Figure 4 shows the bifurcation diagram obtained by continuation of stationary and periodic solutions using the same conditions as in the experiment shown in Figure 2. As can be seen, there is a good qualitative agreement between simulation and experiments. Both model and laboratory reactor pass a region of periodic solutions when the coolant flow is increased slowly from 40 to 120 L/h. Also, the region of existence of periodic solutions is predicted sufficiently well; however, there is a rather big difference between the simulated and the measured temperature maxima. A better qualitative agreement can be achieved by introducing a vapor phase into the model, as shown in ref 31. An important result is the existence of a supercritical and a subcritical Hopf bifurcation point at $\dot{q}_{dos} = 61.98$ L/h and $\dot{q}_{dos} = 110.13$ L/h, respectively. The amplitudes of the periodic solutions near the supercritical Hopf point are small. Therefore, passing this Hopf bifurcation is a safe way to enter the region of periodic solutions. In contrast, the transition from extinguished steady states to periodic solutions by passing the subcritical Hopf point will lead to a sudden onset of oscillations with high temperature peaks and this is hazardous. The reason for this behavior is that high concentrations of hydrogen peroxide accumulate in the reactor on the extinguished branch and react quickly in a strongly exothermic reaction when the Hopf point is crossed. The transition from extinguished to reactive states can also be critical when the temperature difference between the excited and the extinguished steady states is high and the transition between them occurs in a small interval of coolant flows. Therefore, to perform the experiment depicted in Figure 3 it is also important to elaborate a safe start-up procedure in advance by model calculations to prevent temperature overshoots and thermal runaway. Figure 5 shows a safe and a hazardous start-up procedure for this experiment. The start-up can be done safely when the heating power is set high above the desired value ($P_{heat} = 600$ W) at first. Then the dosing is turned on. After a steady state has established, the heating power is diminished to the desired level ($P_{heat} = 150$ W). The start-up is hazardous, if the heating power is low from the beginning ($P_{heat} = 150$ W), because the accumulation of hydrogen peroxide is promoted.

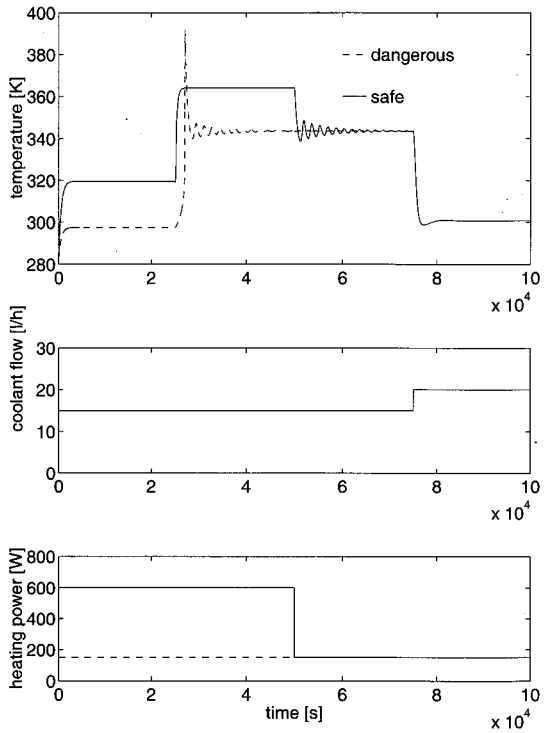

Figure 5. Numerical results: safe and dangerous start-up procedure of the CSTR; initial conditions (weight fractions) before dosing is turned on, $w_{CH_3CH_2OH} = 0.23$, $w_{cat} = 0.02$; weight fractions in dosing, $w_{H_2O_2,dos} = 0.06$, $w_{CH_3CH_2OH,dos} = 0.10$, $w_{cat,dos} = 0.0075$; other conditions: $T_{dos} = 24.0$ °C, $T_{cool,in} = 13.5$ °C, $T_{amb} = 24.0$ °C, $N_{stirr} = 500$/min; $t = 0-25000$ s, $\dot{q}_{dos} = 0$ L/h, $t = 25000-100000$ s, $\dot{q}_{dos} = 10.0$ L/h.

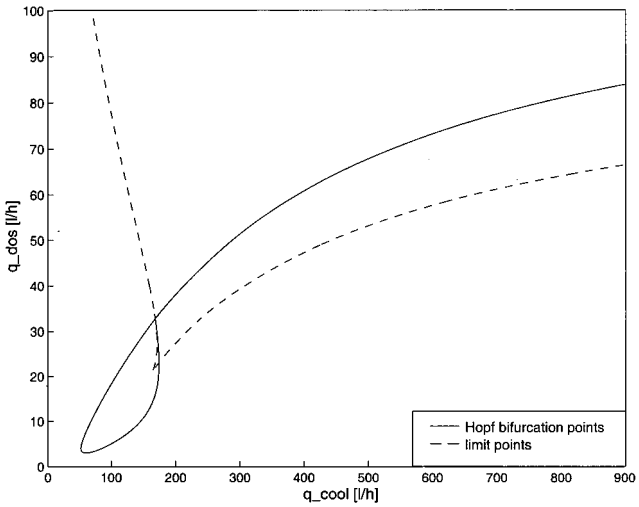

Figure 6. Numerical results: location of Hopf (solid line) and limit points (saddle-node bifurcations) (dashed line) in a two-dimensional parameter plane. Weight fractions in dosing: $w_{H_2O_2,dos} = 0.10$, $w_{CH_3CH_2OH,dos} = 0.10$, $w_{cat,dos} = 0.02$; other conditions, $T_{dos} = 15.0$ °C, $T_{cool,in} = 4.83$ °C, $T_{amb} = 21.7$ °C, $N_{stirr} = 500$/min, $P_{heat} = 1600$ W.

Regions of oscillations and bistability can be determined by a two-parameter continuation of Hopf points and limit points (saddle-node bifurcations). Figure 6 shows the results obtained in the two-parameter plane defined by the volumetric coolant flow $\dot{q}_{cool}$ and the volumetric feed flow $\dot{q}_{dos}$. At low feed flows only one steady state exists. At higher feed flows an oscillating region occurs which is limited by two Hopf bifurcation points. The experiment shown in Figure 2 is performed in this region under similar conditions. Above $\dot{q}_{dos} \approx 21$ L/h two saddle-node

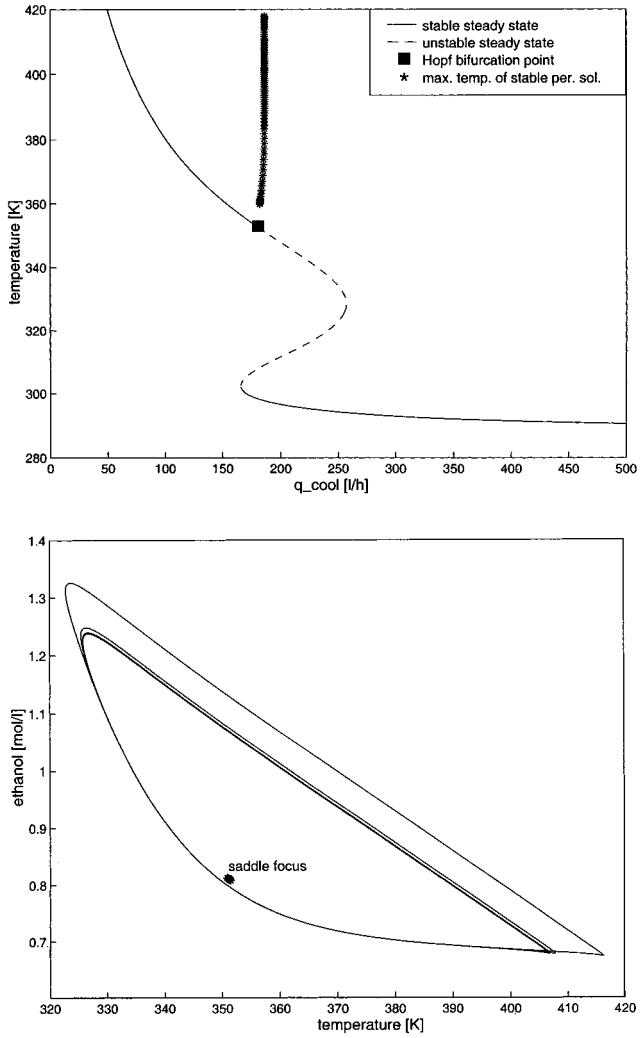

Figure 7. (a) Numerical results: one-dimensional section horizontally across the bifurcation diagram depicted in Figure 6 at $\dot{q}_{dos} = 35$ L/h. (b) Numerical results: location of the limit cycle and the saddle focus in the temperature−ethanol parameter plane just before collision.

bifurcations emerge in addition to the two Hopf bifurcations. Further increasing the feed flow makes one Hopf point vanish at $\dot{q}_{dos} \approx 34$ L/h by collapsing with a saddle-node bifurcation at a Takens−Bogdanov point. At higher dosing rates only one Hopf bifurcation exists, which is located within a region of bistability. Figure 7a shows a bifurcation diagram obtained at constant feed ($\dot{q}_{dos} = 35$ L/h). In this case, a hysteresis of three steady states is found between $\dot{q}_{cool} = 165.8$ L/h and $\dot{q}_{cool} = 257.0$ L/h. There is still a branch of periodic orbits which bifurcates from a supercritical Hopf point at $\dot{q}_{cool} = 180.7$ L/h. However, the temperature maxima as well as the periods of the oscillations increase very steeply in a small region of coolant flows until the limit cycles vanish abruptly without any further participation of a Hopf or a saddle-node bifurcation. These results indicate the existence of a homoclinic orbit formed by collision of the limit cycle with the saddle focus. In Figure 7b the limit cycle and the saddle focus are shown in a two-parameter plane formed by the temperature and the ethanol concentration. A similar situation was already discussed for a single exothermic first-order reaction in a CSTR.[32]

The dynamic behavior of the CSTR becomes even more complex if ethanal is an additional educt. In this case, period-doubling sequences to chaos are found. Beginning with an extinguished steady states near the subcritical Hopf bifurcation and adding ethanal to the feed, we characterized the sequence

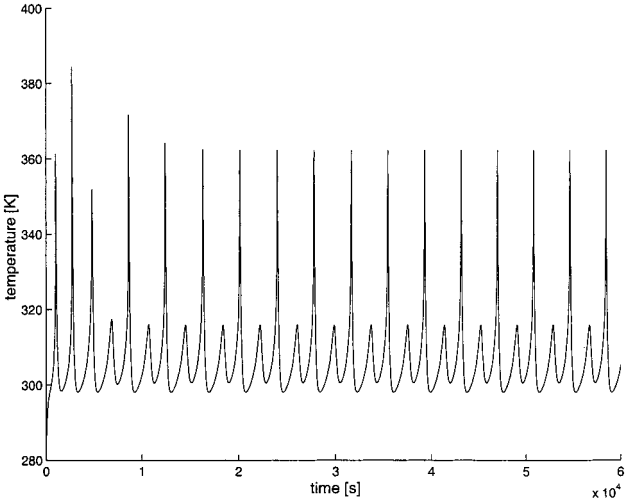

Figure 8. Numerical results: period-2 oscillations. Conditions: weight fractions in dosing, $w_{H_2O_2,dos} = 0.10$, $w_{CH_3CH_2OH,dos} = 0.10$, $w_{CH_3CHO,dos} = 0.0625$, $w_{cat,dos} = 0.02$; other conditions, $T_{dos} = 15.0$ °C, $T_{cool,in} = 4.83$ °C, $T_{amb} = 21.7$ °C, $N_{stirr} = 500$/min, $\dot{q}_{dos} = 5.93$ L/h, $\dot{q}_{dos} = 150$ L/h, $P_{heat} = 1600$ W.

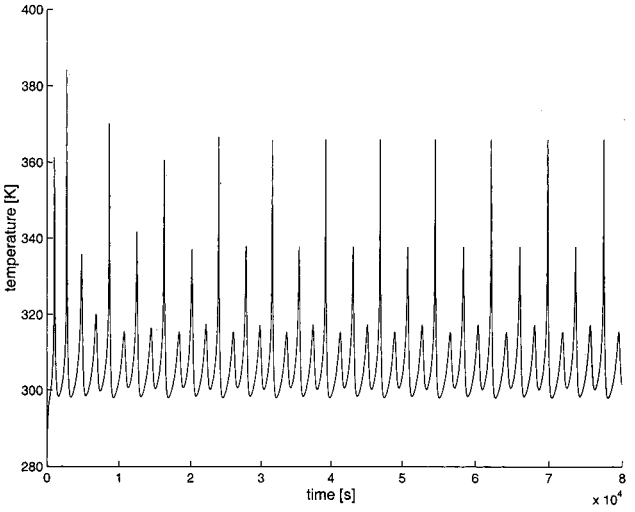

Figure 9. Numerical results: period-4 oscillations. Conditions: $w_{CH_3CHO,dos} = 0.0623$; all other parameters are the same as those in Figure 8.

TABLE 2: Observed States with Feed Stream Containing Ethanal at Different Weight Fractions $w_{CH_3CHO,dos}$. All Other Conditions as Those in Figure 8

$w_{CH_3CHO,dos}$	dynamical state
0.0	steady state
0.061 00	period-1
0.061 50	period-2
0.061 55	period 4
0.061 70	chaos
0.062 00	period-3
0.062 05	chaos
0.062 15	period-5
0.062 20	chaos
0.062 30	period-4
0.062 50	period-2
0.064 00	period-2
0.065 00	period-1

of dynamical states which is summarized in Table 2. Figures 8, 9, and 10a show period-2, period-4, and aperiodic oscillations, respectively. We investigate the attractor using Poincaré sections and one-dimensional maps to prove the deterministic nature of the observed aperiodicity (Figure 10b−d). The one-dimensional map shows a curve with extrema, which is characteristic for

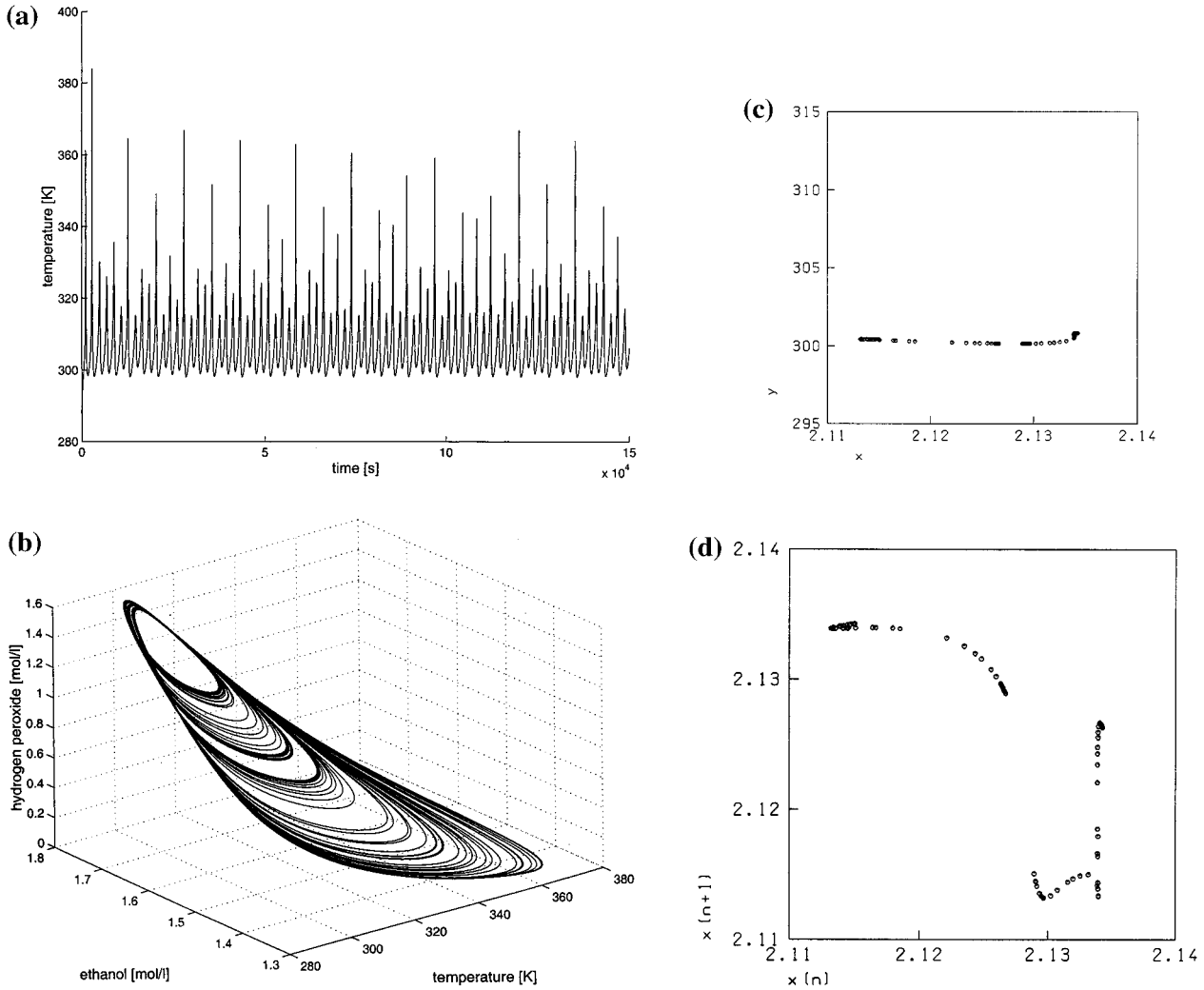

Figure 10. (a) Numerical results: aperiodic oscillations. Conditions: $w_{CH_3CHO,dos} = 0.0622$; all other parameters are the same as those in Figure 8. The deterministic origin of the aperiodicity is evidenced by Figures 10b−d. (b) Numerical results: original attractor, the variables temperature T, concentration of ethanol, and concentration of hydrogen peroxide are shown. (c) Numerical results: Poincaré section obtained from the attractor depicted in Figure 10b. (d) Numerical results: one-dimensional map constructed from the Poincaré section (Figure 10c). The one-dimensional map shows an extrema, which is characteristic for deterministic chaos reached by a period doubling sequence.

deterministic chaos originating from period doubling. We further evaluate the spectrum of Lyapunov exponents from the system of differential equations according to the method described by Wolf, Swift, Swinney, and Vastano.[33] The three largest Lyapunov exponents are found to be $\lambda_1 = 1.052 \times 10{-}4\ s^{-1}$, $\lambda_2 = 0.0$, and $\lambda_3 = -1.001 \times 10{-}3\ s^{-1}$. The positive exponent is a further evidence for the deterministic nature of the observed aperiodicity. According to the Kaplan−Yorke conjecture,[34] the Lyapunov dimension D_L can be calculated from the Lyapunov exponents:

$$D_L = j + \frac{\sum_{i=1}^{j} \lambda_i}{|\lambda_{j+1}|} \tag{19}$$

where

$$\lambda_1 \geq \lambda_2 \geq ... \geq \lambda_{i-1} \geq \lambda_i$$

$$\sum_{i=1}^{j} \lambda_i \geq 0 \sum_{i=1}^{j+1} \lambda_i < 0.$$

The Lyapunov dimension D_L is an upper estimate for the information dimension D_I. In this case we obtained the values 2.11 and 2.28 for the Lyapunov dimension at $w_{CH_3CHO,dos} = 0.0622$ and $w_{CH_3CHO,dos} = 0.0617$, respectively. A fractal dimension, which is above 2.0, is also an indicator for deterministic chaos.

6. Discussion

In the present study the iron(III)-catalyzed oxidation of ethanol with hydrogen peroxide is investigated experimentally as well as by model calculations. This reaction is an interesting example to study the consequences of nonlinear behavior in the context of process performance and process design.

We extended previous work[22] by investigation of parameter changes on the system dynamics. We characterized steady states with high and low conversion rates of ethanol, which are separated by a region of periodic oscillations. The region of oscillations is limited by a supercritical Hopf bifurcation at low coolant flows and a subcritical Hopf bifurcation at high coolant flows. The hard generation of a limit cycle at the subcritical Hopf point is a source of danger. At this bifurcation the reaction "ignites" when the coolant flow is decreased from the branch of steady states with low conversion (extinguished steady state). On this branch of steady states educt species accumulate. When the oxidant hydrogen peroxide is decreased in the feed the subcritical Hopf bifurcation changes into a supercritical bifurca-

tion where the oscillations start with slowly increasing amplitudes. The model calculations overestimate the amplitudes of the temperature oscillations. This could be due to the neglection of the gas phase and the reflux condensor. Experimentally, the boiling point of the reaction solution can be reached in the oscillating region and on the branch of reactive steady states at low coolant flows.[31] The boiling point T_s is of course an upper limit in temperature, which cannot be exceeded experimentally as long as the liquid and the gas phase coexist at atmospheric pressure. In the experiment (Figure 2) the oscillating region is smaller than found by the model calculations. This effect can be explained by the simplifications of the model and the great sensitivity of the location of the subcritical bifurcation on the temperature of the coolant influx.

Guided by continuation studies in the one- and two-parameter space we further found conditions where a nonoscillatory transition between the reactive and extinguished branch of steady states takes place. Working near such a steep transition in temperature may be critical on a technical scale and may afford special care for safe performance of the process. Attention must also be given to start-up or shut-down procedures when exothermic reactions are performed in a CSTR. When the heating power is chosen too low during the start-up the resulting low conversion rate leads to accumulation of educt, which can be dangerous when any further parameter changes are performed. Another hazardous start-up can occur when the amount of catalyst is chosen to be too low before the dosing is turned on.[14]

Besides the existence of monostability and period-1 oscillations, bistability, homoclinic orbits, oscillations of higher periods, and deterministic chaos are found in the model calculations. Starting from the parameter set corresponding to the experiment shown in Figure 2 bistability of stable steady states occurs at high rates of dosing (see Figure 6). Figure 6 is similar to the so called cross-shaped diagrams known from isothermal nonlinear systems.[35] The oscillatory region and the bistability are located on opposite sites of the crossing lines of bifurcation points. At the other pair of sites only one stable steady states exists.

Using a coolant flow slightly above the subcritical Hopf bifurcation (similar conditions as in Figure 2) and adding ethanal to the feed, complex periodic and chaotic states can be detected in narrow parameter ranges. The dimension of these chaotic states is comparable to low dimensional chaos found in isothermal nonlinear systems such as the Belousov−Zhabotinsky reaction.[36] The chaotic states are reached via period-doubling sequences. Within the chaotic region periodic states occur. The whole bifurcation scenario is similar to the behavior of the logistic map[37] and has been characterized in many nonlinear systems, such as chemical reactions,[36] Rayleigh−Bénard convection,[38] and driven electronic circuits.[39]

Acknowledgment. The authors thank the German Bundesministerium für Bildung und Forschung for financial support. We further thank Dr. A. F. Münster from the University of Würzburg for construction of the Poincaré section and the one-dimensional map.

Appendix

The heat transfer from the reaction mixture to the coolant is described by (see eq 18):

$$(UA)_{cool}(T - T_{cool,in}) \tag{20}$$

where T is the reactor temperature, $T_{cool,in}$ is the inlet temperature of the coolant water, and $(UA)_{cool}$ is the overall heat transfer coefficient. The overall resistance of the heat transfer $1/(UA)_{cool}$ is composed of the four resistances R_a, R_b, R_c, and R_d:[40]

$$(UA)_{cool} = \frac{1}{R_a + R_b + R_c + R_d} \tag{21}$$

R_a describes the diffusive and convective heat transfer from the bulk of the reactor to the outer surface of the cooling coil. R_b signifies the resistance due to the thermal conductivity of the steel of the cooling coil. R_c specifies the heat transfer resistance between the inner surface of the cooling coil and the bulk of the coolant water. Finally, R_d describes the heat removal by the coolant. The resistances depend on the geometry of the cooling coil, the thermal conductivities of the reaction mixture, the coolant, and the material of the cooling coil, for example. R_d is of special interest for our investigations because it is a function of the coolant flow $\dot{q}_{cool}$ which is used as a bifurcation parameter.

$$R_d = \frac{1}{\dot{q}_{cool}\rho_{cool}c_{p,cool}\left[1 - \exp\left(-\frac{\alpha_{cool}A_w}{\dot{q}_{cool}\,\rho_{cool}c_{p,cool}}\right)\right]} \tag{22}$$

ρ_{cool} and $c_{\rho,cool}$ are the density and the specific heat capacity of the coolant water. These quantities are evaluated by correlations given in ref 24. α_{cool} denotes the heat transfer coefficient at the coolant side of the coil, and A_w is the surface of the cooling coil.

References and Notes

(1) Razón, L.; Schmitz, R. *Chem. Eng. Sci.* **1987**, *42*, 1005 and references therein.
(2) Wirges, H.-P. *Verfahrenstechnik* **1983**, *17*, 489 and references therein.
(3) Brandes, H. In *Grundlagen der chemischen Prozessregelung*; Oppelt, W., Wicke, E., Eds.; Oldenbourg: München, 1964; p 65.
(4) Hugo, P. *Proceedings of the European Symposium on Chemical Reaction Engineering* **1968**, *4*, 459.
(5) Bush, S. F. *Proc. R. Soc.* **1969**, *309*, 1.
(6) Baccaro, G. P.; Gaitonde, N. Y.; Douglas, J. M. *AIChE J.* **1970**, *16*, 249.
(7) Beusch, H.; Fieguth, P.; Wicke, E. *Chemie-Ing.-Techn.* **1972**, *44*, 445.
(8) Schmitz, R. A.; Bautz, R. R.; Ray, W. H.; Uppal, A. *AIChE J.* **1979**, *25*, 289.
(9) Chang, M.; Schmitz, R. A. *Chem. Eng. Sci.* **1975**, *30*, 21.
(10) Heemskerk, A. H.; Dammers, W. R.; Fortuin, J. M. H. *Chem. Eng. Sci.* **1980**, *35*, 439.
(11) Wirges, H.-P.; *Chem. Eng. Sci.* **1980**, *35*, 2141.
(12) Dubil, H.; Gaube, J. *Chemie-Ing.-Tech.* **1973**, *8*, 529.
(13) Wittmer, P.; Ankel, T.; Gerrens, H.; Romeis, H. *Chemie-Ing.-Tech.* **1965**, *37*, 392.
(14) Alós, M. A.; Obertopp, T.; Mangold, M.; Gilles, E. D. *Praxis der Sicherheitstechnik* **1997**, *4*, 293.
(15) Morud, J. C.; Skogestad, S. *AIChE. J.* **1998**, *44*, 888.
(16) Douglas, J. M.; Rippin, D. W. T. *Chem. Eng. Sci.* **1966,** *21*, 305.
(17) Seider, W. D.; Brengel, D. D.; Widago, S. *AIChE J.* **1991**, *37*, 1.
(18) Stankiewicz, A.; Kuczynski, M. *Chem. Eng. Process.* **1995**, *34*, 367.
(19) van Heerden, C. *Chem. Eng. Sci.* **1958**, *8*, 133.
(20) Aris, R.; Amundson, N. R. *Chem. Eng. Sci.* **1958**, *7*, 121.
(21) Gilles, E. D.; Hofmann, H. *Chem. Eng. Sci.* **1961**, *15*, 328.
(22) Hafke, C.; Gilles, E. D. *Mess., Steuern, Regeln* **1968**, *11*, 204.
(23) Zlokarnik, M. In *Ullmanns Encyclopädie der technischen Chemie*; Verlag Chemie: Weinheim, 1972; Vol. 2.
(24) Daubert, T. E.; Danner, R. P. *Physical and Thermodynamic Properties of Pure Chemicals Data Compilation*; Hemisphere Publishing: New York, 1989.
(25) Figgis, B. N.; Robertson, G. B. *Nature* **1965**, *205*, 694.
(26) Hafke, C. Dissertation, Universität Stuttgart, Germany, 1972.
(27) Mansfield, J. M.; Pulley, R. A.; Wilson, J. A. *I. ChemE Res. Event* **1995**, 484.

(28) *Verein Deutscher Ingenieure VDI-Wärmeatlas,, Berechnungsblätte für den Wärmeübergang*; VDI, GVC: Düsseldorf, 1994.

(29) Majer, C. *Parameterschätzung, Versuchsplanung und Trajektorienoptimierung für verfahrenstechnische Prozesse*, Dissertation, Universität Stuttgart, 1997.

(30) Mangold, M.; Kienle, A.; Mohl, K. D.; Gilles, E. D. *Chem. Eng. Sci.* **1999**. Manuscript accepted for publication.

(31) Zeyer, K.-P.; Mangold, M.; Obertopp, T.; Gilles, E. D. *Chem. Eng. Sci*. Manuscript accepted for publication.

(32) Uppal, A.; Ray, W. H.; Poore, A. B. *Chem. Eng. Sci.* **1974**, *29*, 967.

(33) Wolf, A.; Swift, J. B.; Swinney, H. L.; Vastano, J. A. *Physica* **1985**, *16D*, 285.

(34) Kaplan, J. L.; Yorke, J. A. In *Lecture Notes in Mathematics*; Peitgen, H. O., Walther, H. O., Eds.; Springer: Berlin, 1979; Vol. 730, p 228.

(35) De Kepper, P.; Boissonade, J. *J. Chem. Phys.* **1981**, *75*, 189. Bar-Eli, K.; Geiseler, W. *J. Phys. Chem.* **1983**, *87*, 3769.

(36) Simoyi, R. H.; Wolf, A.; Swinney, H. L. *Phys. Rev. Lett.* **1982**, *49*, 245. Schneider, F. W.; Münster, A. F. *J. Phys. Chem.* **1991**, *95*, 2130.

(37) Verhulst, P. F. *Correspond. Math. Phys.* **1938**, *10*, 113. May, R. M. *Nature* **1976**, *261*, 459.

(38) Libchaber, A.; Maurer, J. *J. Phys. (Paris) Coll.* **1980**, *41*, C3.

(39) Linsay, P. S. *Phys. Rev. Lett.* **1981**, *47*, 1349.

(40) Obertopp, T.; Alós, M. A.; Mangold, M.; Gilles, E. D. *Automatisierungstechnik* **1999**. Manuscript accepted for publication.